

Self-gated self-supervised ADMM unrolling enables mesoscale high-resolution motion-robust diffusion-weighted imaging

Zhengguo Tan, Patrick A Liebig, Annika Hofmann, Yun Jiang, Vikas Gulani, Frederik B Laun, Florian Knoll

SYNOPSIS & IMPACT

Motivation: The lack of fully-sampled data hinders the developments of advanced deep learning techniques for diffusion-weighted imaging (DWI).

Goal: To develop an efficient self-supervised algorithm unrolling technique for high-resolution DWI.

Approach: We unroll the alternating direction method of multipliers (ADMM) to perform scan-specific self-supervised learning for deep DWI reconstruction.

Results: We demonstrate that (1) ADMM unrolling is generalizable across slices, (2) ADMM unrolling outperforms multiplexed sensitivity-encoding (MUSE) and compressed sensing with locally-low rank (LLR) regularization in terms of image sharpness, tissue continuity and motion robustness, (3) ADMM unrolling enables clinically feasible inference time.

Impact: Our proposed ADMM unrolling enables whole brain DWI of 21 volumes at 0.7 mm isotropic resolution and 10 minutes scan, and shows higher signal-to-noise ratio (SNR), clearer tissue delineation, and improved motion robustness, which make it plausible for clinical translation.

INTRODUCTION

High-dimensional MRI (HD-MRI) is a rapidly advancing field, with examples including MRSI [1], DWI [2], and quantitative parameter mapping [3,4]. State-of-the-art HD-MRI often requires prolonged acquisition times. While accelerated techniques, such as compressed sensing reconstruction, can shorten acquisition, they come with the trade-off of increased computational demands.

The contribution of this work includes:

- We unroll ADMM [5] to perform self-gated scan-specific self-supervised learning for deep DWI.
- We demonstrate the generalizability of the trained ADMM unrolling model.
- We achieve whole-brain 0.7mm DWI with 21 diffusion-encoding directions at 10 minutes scan time.

METHODS

Data Acquisition

Three volunteers and one patient with written informed consent approved by the local ethics committee participated in the study.

Brain DWI at 7T

Three volunteers were scanned at 7T (MAGNETOM Terra) with the mesoscale high-resolution DWI protocol based on NAViEPI [6]: FOV 200 mm, matrix size 286 x 286 x 176, voxel size 0.7 mm $\times 3$, 3-shot interleaved EPI with 2x2-fold acceleration and 5/8 partial Fourier, bandwidth 972 Hz/pixel, TR/TE/ESP 8900/58/1.17 ms, and a total scan time of 10 minutes for 21 volumes (1 non-diffusion-weighted and 20 diffusion-encoded) with the b-value 1000 s/mm $\times 2$.

Prostate DWI at 3T

One patient was scanned at 3T (MAGNETOM Vida) with the clinical prostate DWI protocol utilizing single-shot EPI: FOV 200 mm, matrix size 171 x 114 x 35, slice thickness 4 mm, 2-fold in-plane acceleration, TR/TE 6400/91 ms, and the 3-scan trace mode with b-values 0, 100, 800, and 1600 s/mm $\times 2$ and 97 volumes. ADC was obtained as the average of diagonal tensors, which was fitted from diffusion-weighted images excluding the b-value 1600 s/mm $\times 2$.

Forward Modeling

Joint k-q-slice reconstruction [6] formulates the forward model as,

$$\mathcal{A}(\mathbf{x}) = \mathbf{P} \Sigma \Theta F S \Phi \mathbf{x}$$

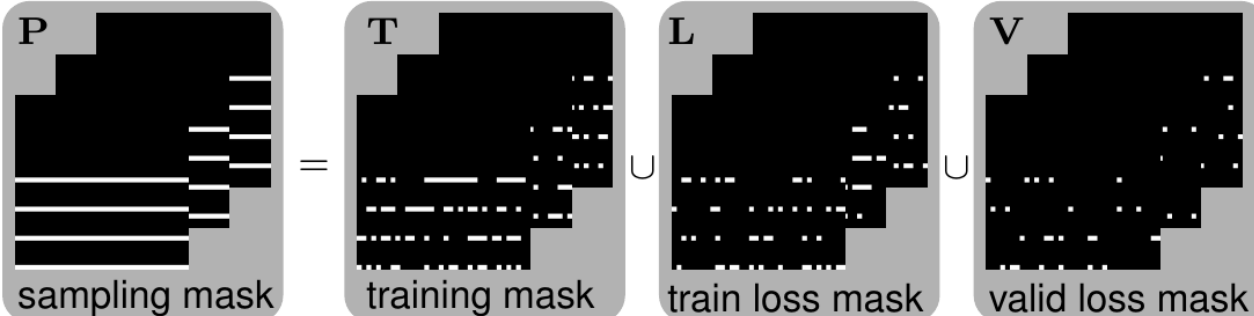
where the multi-band multi-diffusion-weighted images (\mathbf{x}) is mapped to k-space via a chain of linear operators, including the shot-to-shot phase variation (Φ), coil sensitivities (S), 2D FFT (F), multi-band phases ($\Sigma \Theta$), and the undersampling mask (P). With the forward model (\mathcal{A}), the joint reconstruction reads,

$$\text{argmin}_{\mathbf{x}} \| \mathbf{y} - \mathcal{A}(\mathbf{x}) \|_2^2 + \lambda \mathcal{R}(\mathbf{x})$$

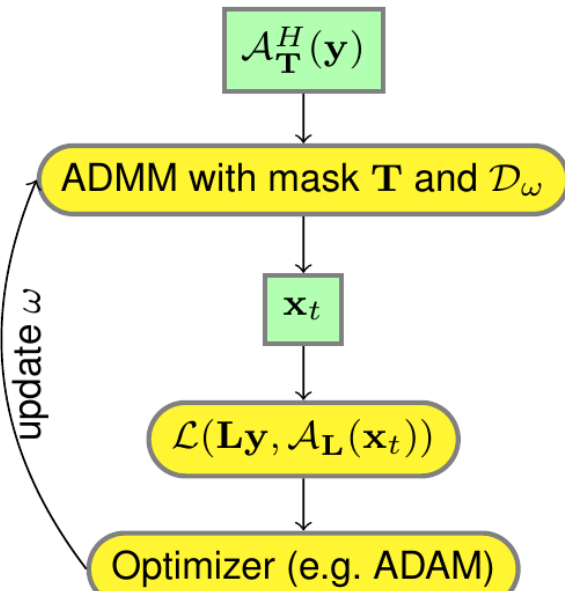
where \mathbf{y} is the measured k-space. The regularization function $\mathcal{R}(\mathbf{x})$ in this work is either nuclear norms of the local spatial-diffusion patches for LLR-regularized reconstruction or the 2D ResNet [7] for unrolled reconstruction. In both cases, we employ ADMM to assure fair comparison.

Self-Gated Self-Supervised ADMM Unrolling

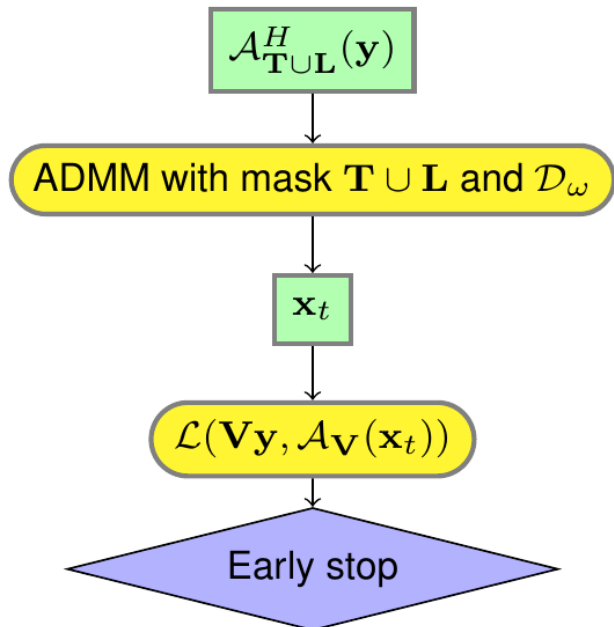
(A) uniform splitting of sampling masks



(B) loop over all repetitions per epoch



(C) validation



(D) spatial-diffusion convolution

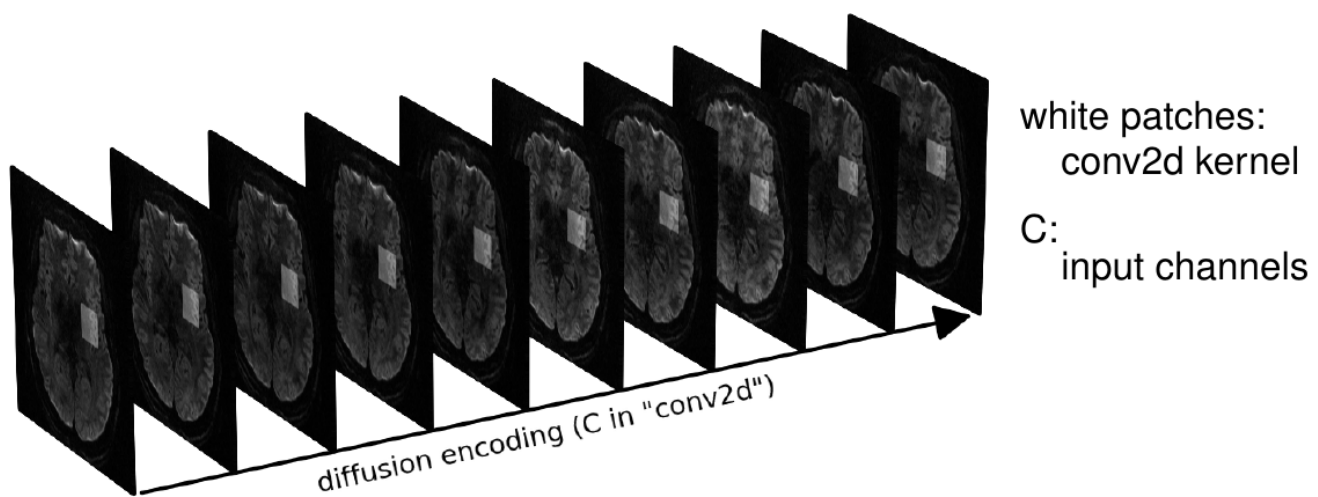


Figure 1. Key components in ADMM unrolling. (A) The sampling mask P was uniformly split into three disjoint sets: the training mask T for the data consistency term during training, the train loss mask L for the loss function calculation during training, and the validation loss mask V for the loss function calculation during validation. (B) and (C) show the flowchart for the training and the

validation, respectively. The ResNet parameters are updated via ADAM during training, but remain fixed during validation. (D) All diffusion-weighted images are input to ResNet in ADMM unrolling.

Inspired by Yaman et al. [8], our proposed ADMM unrolling is scan specific, i.e., the model is trained on one single dataset. The data sampling mask \mathbf{P} in Figure 1 is split into three disjoint sets. Each set consists of 12 repetitions constructed via random uniform sampling of the data mask \mathbf{P} . In each training epoch, every repetition is looped through to update the ResNet parameters ω . Plus, the validation loss is computed after every training epoch to update the minimal validation loss, which, if not reduced for 12 consecutive epochs, terminates the training. The 2D convolution in ResNet is performed in the spatial-diffusion dimension, with the diffusion encoding as the convolution channel. All reconstructions were done on a A100 SXM4/NVLink GPU with 80GB memory (NVIDIA, Santa Clara, CA, USA).

RESULTS AND DISCUSSION

Model Generalizability

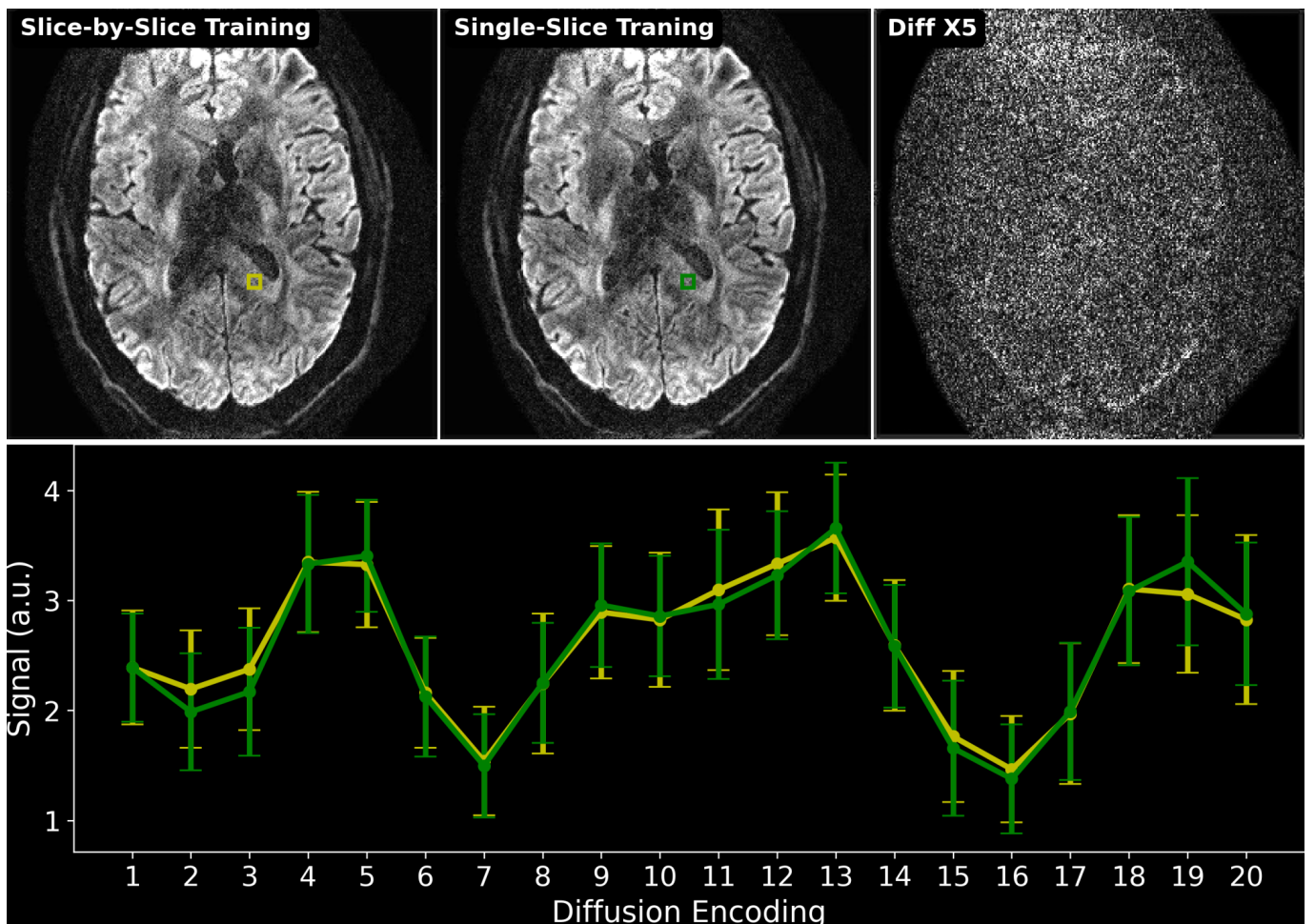


Figure 2. Comparison of two training strategies: (1) slice-by-slice training, where every slice is trained and tested individually; (2) single-slice training, where the unrolled ADMM model is trained on only one slice and tested on all remaining slices. The top-right image shows the absolute difference between the reconstructed single-dir diffusion-weighted images between (1) and (2). The bottom panel plots the mean and standard deviation of the signal within color boxes in the two training strategies. No major qualitative or quantitative difference can be seen.

Figure 2 demonstrates the generalizability of the proposed ADMM unrolling approach, i.e., an unrolled ADMM model trained on one single slice is applicable to all remaining "unseen" slices. The absolute

difference and the plotted mean and standard deviation within the region-of-interest (colored boxes) along all diffusion encoding show no major difference.

Self-Gated Self-Supervised ADMM Unrolling

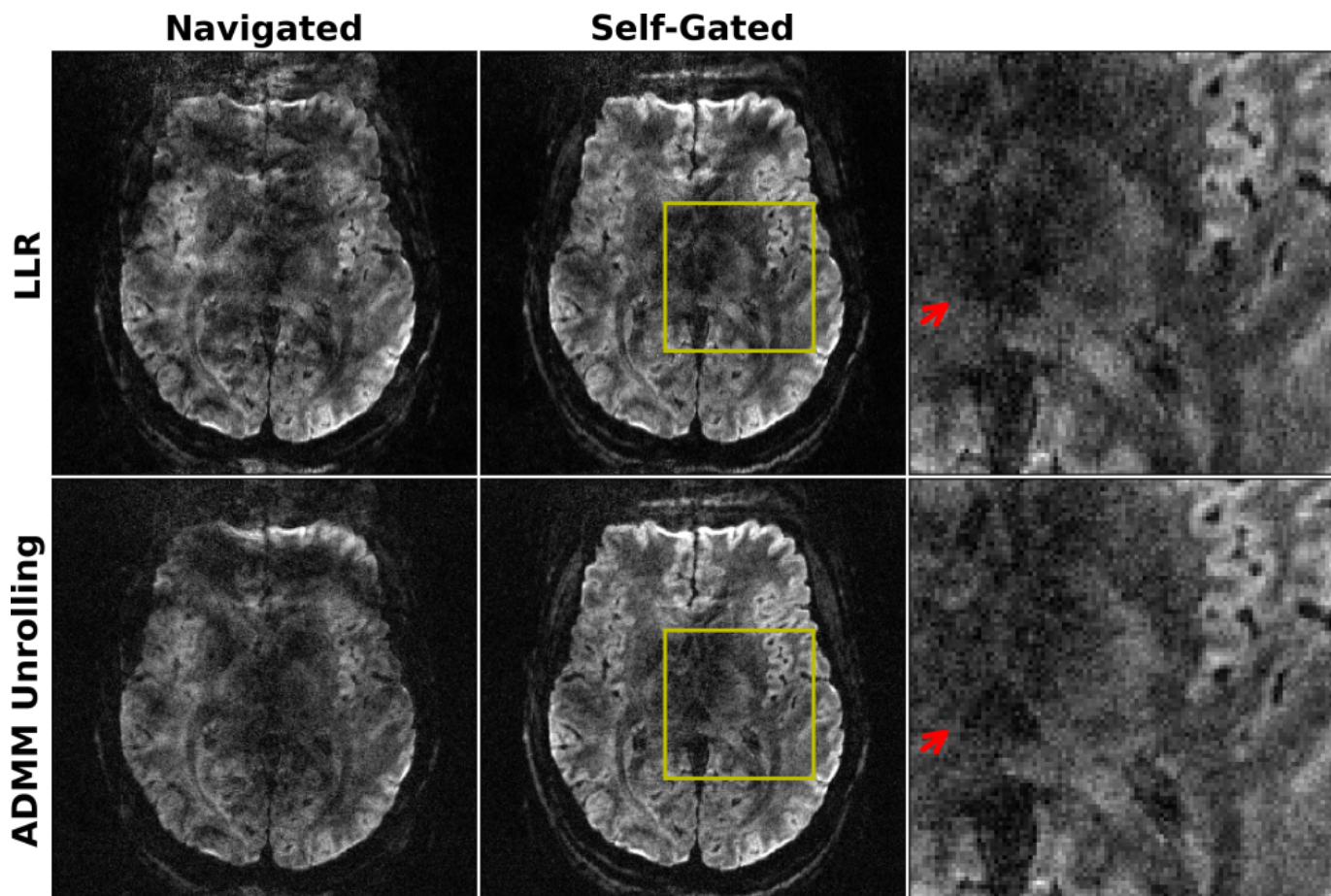


Figure 3. Comparison of (top) LLR and (bottom) ADMM unrolling reconstruction on 0.7mm isotropic resolution DWI with shot phase estimated from (left) navigators and (middle) imaging echoes, respectively. The use of navigators prolongs the total scan time, and thus increases the sensitivity to motion, as shown in navigated reconstruction. The retrospectively self-gated reconstruction discards navigators, and renders sharper diffusion-weighted images. Compared to LLR, unrolled ADMM is advantageous in resolving clearer tissue boundaries in diffusion-weighted images.

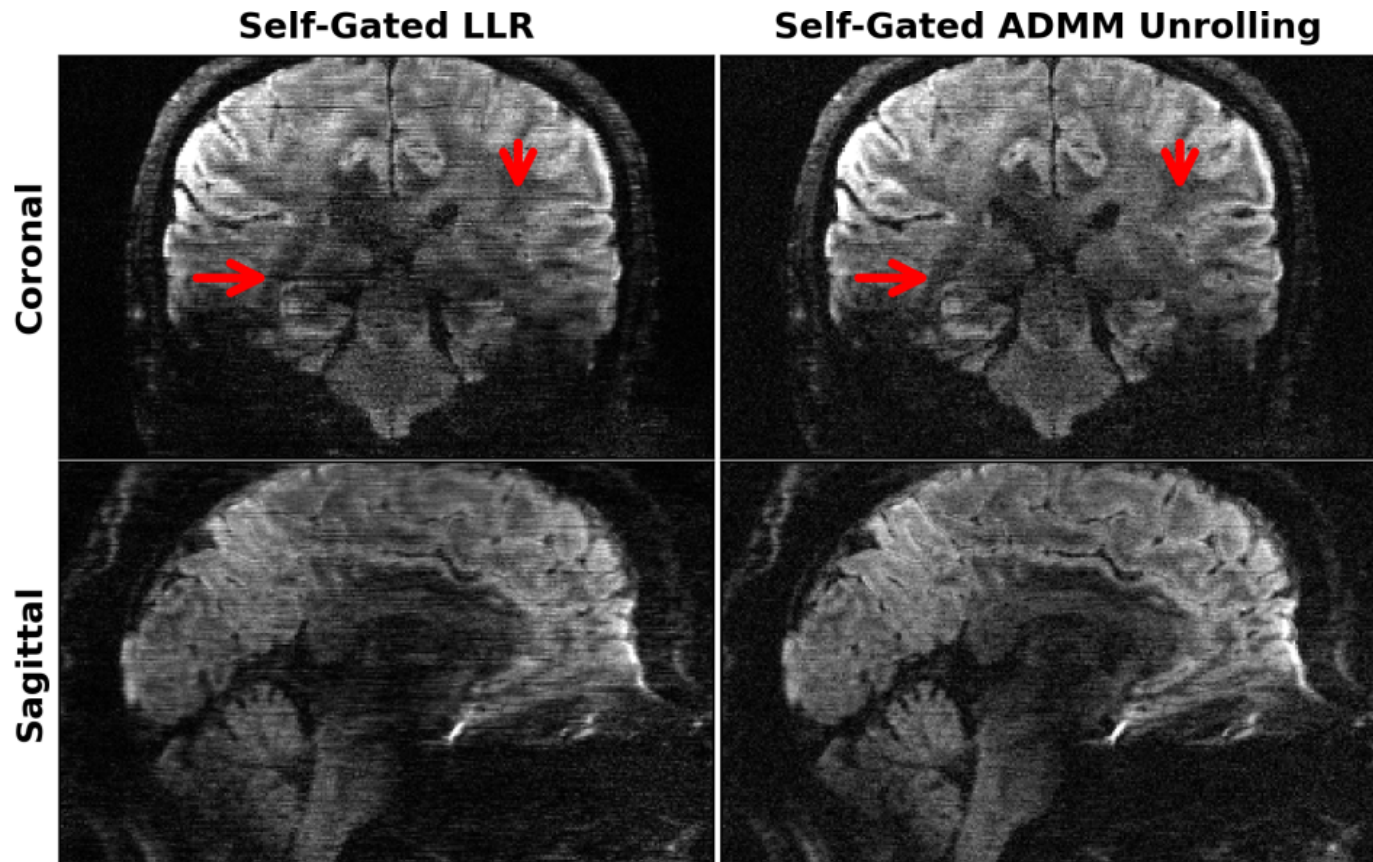


Figure 4. Single-direction diffusion-weighted images at 0.7mm isotropic resolution as reconstructed by retrospectively self-gated (left) LLR and (right) ADMM unrolling in (top) the coronal and (bottom) the sagittal views, respectively. The same diffusion direction as in Figure 3 is chosen for display. ADMM unrolling reduces phase ambiguities in the shot-combined reconstruction, thereby rendering clearer tissue delineation and reducing stripping artifacts (as indicated by the red arrows).

Figures 3 demonstrates the efficacy of the self-gated self-supervised ADMM unrolling reconstruction. The single-direction diffusion-weighted images with accidental motion are displayed. As the acquisition of navigators increases the total scan time, resulting in higher sensitivity to accidental motion, as shown by artifacts in the navigated reconstructions. Self-gated ADMM unrolling exhibits much clearer tissue delineation in reconstructed diffusion-weighted images. Figure 4 demonstrates again that the model generalizes well across slices and shows much reduced stripping artifacts in reformatted views than LLR. The inference of every slice takes only about one minute, whereas the LLR reconstruction takes about 48 minutes per slice.

Prostate DWI

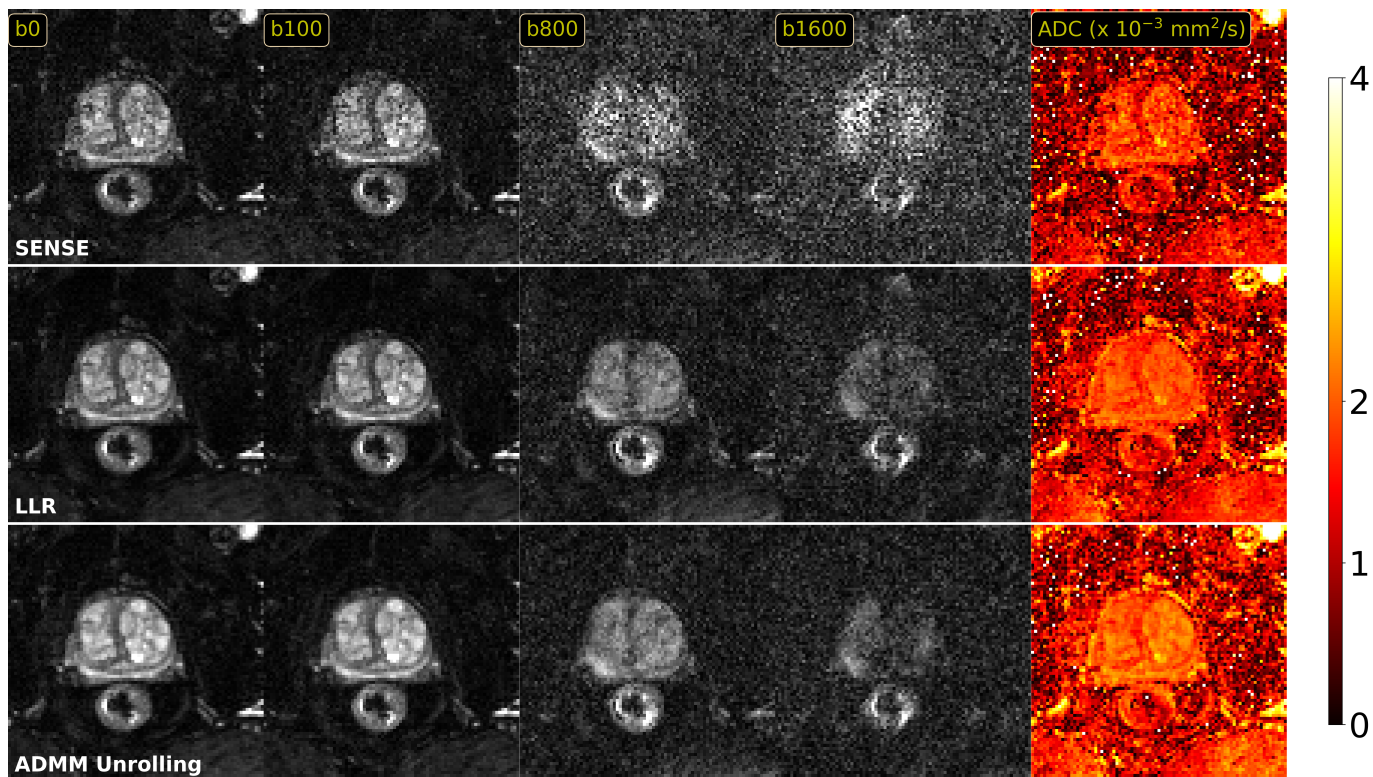


Figure 5. Comparison of reconstructions for prostate DWI: parallel imaging as SENSE, compressed sensing with LLR regularization, and ADMM unrolling. b0, diffusion-weighted images at different b-values, and ADC maps are displayed from left to right. Unlike clinical protocols which may involve the use of dedicated filtering, the ADC maps were fitted directly from reconstructed diffusion-weighted images and displayed without filtering. Both LLR and ADMM unrolling show strong denoising capabilities.

Figure 5 shows preliminary results on prostate DWI reconstruction. While the clinical protocol with online reconstruction may have internal filtering, our ADC maps were fitted directly from reconstructed diffusion-weighted images. Both LLR and ADMM unrolling show strong denoising than SENSE [9]. ADMM unrolling illustrates slightly better tissue contrast in the ADC map.

CONCLUSION

We proposed a self-gated self-supervised learning reconstruction for high-resolution and motion-robust DWI. Based on the mechanism of data splitting (cross validation), our proposed ADMM unrolling requires only one slice for training and is generalized cross-slice.

REFERENCES

- [1] Brown TR, Kincaid BM, Uğurbil K. NMR chemical shift imaging in three dimensions. Proc Natl Acad Sci USA 1982;79:3523-3536.
- [2] Jones DK. Diffusion MRI: Theory, methods, and applications. Oxford University Press 2010.
- [3] Doneva M, Boernert P, Eggers H, Stehning C, Senegas J, Mertins A. Compressed sensing for magnetic resonance parameter mapping. Magn Reson Med 2010;64:1114-1120.
- [4] Ma D, Gulani V, Seiberlich N, Liu K, Sunshine JL, Duerk JL, Griswold MA. Magnetic resonance fingerprinting. Nature 2013;495:187-192.

- [5] Boyd S, Parikh N, Chu E, Peleato B, Eckstein J. Distributed optimization and statistical learning via the althernating direction method of multipliers. *Foundations and Trends in Machine Learning* 2010;3:1-122.
- [6] Tan Z, Liebig PA, Heidemann RM, Laun FB, Knoll F. Accelerated diffusion-weighted magnetic resonance imaging at 7 T: Joint reconstruction for shift-encoded navigator-based interleaved echo planar imaging (JETS-NAViEPI). *Imaging Neuroscience* 2024;2:1-15.
- [7] He K, Zhang X, Ren S, Sun J. Deep residual learning for image recognition. in *IEEE Conference on Computer Vision and Pattern Recognition (CVPR'16)*. 2016:770-778.
- [8] Yaman B, Hosseini SAH, Akçakaya M. Zero-shot self-supervised learning for MRI reconstruction. in *10th International Conference on Learning Representations (ICLR'10)*. 2022.
- [9] Pruessmann KP, Weiger M, Boernert P, Boesiger P. Advances in sensitivity encoding with arbitrary k-space trajectories. *Magn Reson Med* 2001;46:638-651.